TSAR

TOPOLOGICAL **S**OLITONS IN **A**NTIFE**R**ROICS

Document title **Document type** **Dissemination level**	**D1.3 Calculations on interfacial DMI + Phase diagrams** Report Public	**AUTHOR** **Due date** **Ref.**	Manuel Bibes 31/10/2022 D1.3
Deliverable description	Initial		

Project	TSAR	**Grant number**	964931
Call identifier **Work Package**	FETOPEN 2018-2019-2020-01 Topological AntiferroMagnetic textures		
WP N°	WP1	**WP leader**	CNRS
Coordinator **Project manager** **Project start date** **Project duration**	Michel Viret Marie-Astrid Cavrois-Desmier 01/05/2021 48 months		

Distribution List

Partner n°	Organization name (Short name)	Name	Country
	European Commission (EU)- Project Officer	Adelina Nicolaie	Belgium
1	Commissariat à l'Energie Atomique (CEA)	Michel Viret	France
2	CNRS node (CNRS)	Manuel Bibes	France
3	University College London (UCL)	Pavlo Zubko	England
4	Centrale-Supelec (CS)	Brahim Dkhil	France
5	ICN2 Barcelona (ICN2)	Gustau Catalan	Spain
6	Université de Liège (ULIEGE)	Philippe Ghosez	Belgium
7	IP-ACSR Prague (IP-ACSR)	Jiří Hlinka	Czech Republic
8	THALES (THALES)	Romain Lebrun	France

This project has received funding from the European Union's Horizon 2020 research and innovation programme under grant agreement No 964931

1) Spin-current driven Dzyaloshinskii-Moriya interaction in $BiFeO_3$ from first-principles

The stability of magnetic solitons depends on the balance between the magnetic exchange, the magnetic anisotropy and the Dzyaloshinskii-Moryia (DM) interactions. In metals, this interaction is mediated by the presence of a heavy magnetic element, which generates a large spin orbit coupling and therefore enhances the DM interaction. This mechanism is well controlled in metals and is usually understood based on the Levy and Fert (LF) model[1].

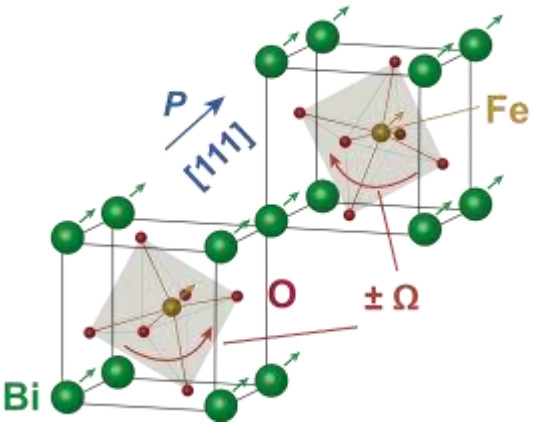

Figure 1: Structure of BiFeO3 sketched in cubic representation. *Compared to the cubic perovskite structure, several peculiarities in BFO occur: The Oxygen octahedra are tilted in antiphase (denoted as ±Ω) and both, Bi and Fe are displaced in the [111] direction (shown as small green arrows at the Bi sites and small golden arrows at the Fe sites). Due to these distortions, a large polarization P along the [111] occurs. This polarization can be directly connected to the Dzyaloshinskii-Moriya interaction, which is responsible for*

Recently, we have shed the light on the importance of internal electric fields in the presence of the DM interaction and have further shown that when this electric field was created by a laser pulse, it could create an antiferromagnetic (AFM) skyrmion at the pico-second time scale[2]. In that case, the DM interaction is directly proportional the electric field and has a symmetry that resembles the one of the Rashba-DM interaction[3]: It is maximum in a plane perpendicular the electric field direction and cancels out in the direction of the electric field.

In multiferroics, internal electric fields play a major role since they are responsible for the polarization. Especially, in the multiferroic $BiFeO_3$, the polarization is rather large up to $90\mu C/cm^{-2}$ in the R3c phase. In this material, the origin of the DM interaction is particularly rich. The DM vector has 2 components: The first one is perpendicular to the polarization and has therefore a Rashba DM-like symmetry while the other component is perpendicular to it and has a symmetry similar to the one of the LF model in metals. They are called the convert spin current (SC) and the spin-canting DM interaction, respectively.

The SC DM interaction is responsible for the stabilization of the AFM spin spiral in BFO while the spin-canting DM interaction is responsible for its weak ferromagnetic (FM) moment. Although these interactions have been known for decades, they have never been quantified based on density functional theory calculations (DFT). Calculating these contributions is challenging with our DFT method based on the generalized Bloch theorem because our approach has been developed to study metals in high symmetry phases such as simple cubic or face centered cubic and not insulator in complex phases such as the R3c phase of bulk BFO.

To mitigate the risks, we have followed 3 approaches.

We have calculated the magnetic exchange and the DM interaction for BFO R3c using an effective Hamiltonian based on Wannier functions[4], our traditional approach as implemented in FLEUR[5] and our new implementation of the Generalized Bloch theorem in Abinit (particularly suited for multiferroic oxides in complex geometries). On the one hand, the two first approaches give similar results. On the other hand, our new implementation of the generalized Bloch theorem gives unphysical results. Although this methodological development seems of secondary importance, it will allow the study of complex metal-oxide interfaces which are central to this project.

As this methodological development is delayed, we have explored both BFO and the metal-oxide interfaces based on our traditional approach[6]. Figure 2 shows the symmetry differences between the Levy and Fert model and the spin current model (Fig. 2 panel (a) and (b)) and the results of our DFT calculations (black points) as

This project has received funding from the European Union's Horizon 2020 research and innovation programme under grant agreement No 964931

well as the fit to both the Levy and Fert model (blue line) and the spin current model (red line). In both models, the DM energy is written as:

$$E_{DM} = \boldsymbol{D_{ij}} \cdot (\boldsymbol{M_i} \times \boldsymbol{M_j})$$

Where $\boldsymbol{D}_{ij}$ is the DM vector and $\boldsymbol{M}_i$ is the magnetic moment on site i. The amplitude and the symmetry of the DM vectors differentiate between the 2 models. In the Levy and Fert model (Fig. 2(a)), $\boldsymbol{D}_{ij}$ is directly proportional to the spin orbit coupling (SOC) of the heavy element (blue sphere). Its direction is fixed by the crystal symmetry. In the spin current model, $\boldsymbol{D}_{ij} = \boldsymbol{P} \times \boldsymbol{e}_{ij}$ where $\boldsymbol{P}$ is the polarization direction and $\boldsymbol{e}_{ij}$ is the unit vector between the magnetic sites I and j. Its amplitude is maximum perpendicularly to both $\boldsymbol{P}$ and $\boldsymbol{e}_{ij}$ and this term should cancel exactly in the direction of $\boldsymbol{P}$. As the polarization directly depends on structural distortions, it naturally couples the structure of the multiferroic material and the magnetic state. To explore and quantify both contributions, we have calculated the SOC contribution to an AFM spin spiral propagating along high and low symmetry lines in bulk BFO R3c as shown in figure 2(c). For this calculation, the polarization lies along the [111] direction. The SOC contribution shows a strong contribution in the $[1\bar{1}0]$ and the $[11\bar{2}]$ directions that correspond to the directions of the so-called type 1 and type 2 spin spirals. Surprisingly, the SOC contribution is also strong in the $[11\bar{1}]$ direction which is not perpendicular to $\boldsymbol{P}$. Furthermore, the SOC contribution combined with the magnetic exchange interaction reveals that both the type 1 and 2 spin spirals are degenerate and could occur simultaneously in bulk BFO R3c. Finally, the SOC contribution cancels out in the [111] direction.

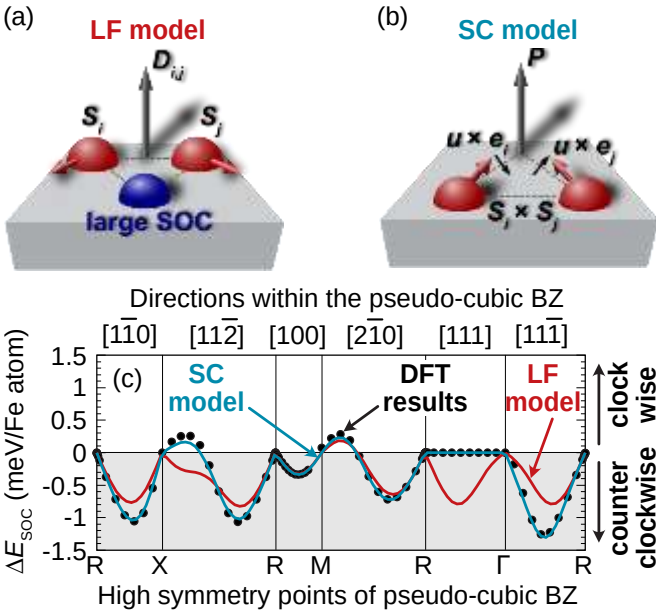

Figure 2: Dzyaloshinskii-Moriya interaction (DM interaction) in $BiFeO_3$. *(a) Model of Levy and Fert (LF) to describe the Dzyaloshinskii-Moriya interaction. Two magnetic atoms $\boldsymbol{S_i}, \boldsymbol{S_j}$ are interacting via a heavy metal atom hosting large spin-orbit coupling (SOC). The triangle between the three atoms defines the DM vector $\boldsymbol{D}_{ij}$. (b) Converse spin-current (SC) model. In systems with a polarization $\boldsymbol{P}$, the spin-current vector $\boldsymbol{u} \times \boldsymbol{e}_{i,j}$ is perpendicular to the direction of polarization. (c) Energy contribution due to spin-orbit coupling ΔESOC to the energy dispersion of spin spirals along different directions within the pseudo-cubic Brillouin zone. Points show calculated energies from density functional theory (DFT), the red line corresponds to the LF model, the blue line corresponds to the SC model. Positive (negative) values prefer clockwise (counterclockwise) sense of rotation of non-collinear states.*

To interpret the data, the SOC contribution was fitted to both the LF (red curve) and the SC (blue curve) models. For the LF model, the Oxygen sites were used as the heavy element site. The LF model shows a relatively good agreement on the [111] direction where it predicts a non-zero contribution which is incompatible with the data. On the other hand, the SC model shows an excellent agreement for all directions including an exact zero contribution in the [111] direction. The SC model can also reproduce correctly the symmetry of the DM interaction in multiferroics. The DM interaction obtained is of the order of 400 μeV/Fe which is in very good agreement with previous experimental estimations[7] but also very small as compared to what could be expected in metals.

This project has received funding from the European Union's Horizon 2020 research and innovation programme under grant agreement No 964931

2) Phase diagram in bulk $BiFeO_3$ using the magneto-electric generalized DM interaction

Usually, magnetic skyrmions are obtained in artificial heterostructures by engineering their interface properties[1,8]. The basic relevant interaction is thus the DM interaction that stems from coupling between magnetic atoms in the interface electrical built-in field. It is therefore of the same nature as the more general magnetoelectric interaction expressing the gain in energy in presence of an internal electric field, or polarization, when magnetism is non-collinear [9–11]: $E_{ME} = \gamma_{ME} \sum \vec{P}.(\overrightarrow{e_{ij}} \times (\vec{S_i} \times \vec{S_j}))$ with γ_{ME} the inhomogeneous ME constant, P the polarization, e_{ij} the vector linking nearest neighbours and $S_i x S_j$ the cross product of neighbouring spins. Therefore, magneto-electric materials intrinsically possess in the bulk the relevant interaction for generating skyrmions with the extra functionality that unlike interfaces, it can be toggled by changing the electrical polarization.

We have chosen to model antiferromagnetic textures using an atomic simulation because as soon as the basic micromagnetic cell is larger than the actual individual spins, magnetization is no longer constant (and falls close to zero). Our code is dynamical in nature where the two AF sublattices are described by a set of two coupled Landau-Lifshitz-Gilbert (LLG) precession equations[12–14]. Any perturbation results in coupled motion of individual spins and the existence of damping makes the system reach a stable static state after some time. This is generally quite heavy on calculation time if one wants to extend it to simulating a reasonable volume, say 10^6 spins. Here, a specific program was written to process the time evolution using the LLG equation in parallel on GPU.

The code has first been tested on relaxed bulk BFO using its intrinsic parameters[7] and we do find that the stable state is that of an AF cycloid with a pitch of 63 nm. All basic validations being done, we want here to study under which conditions a skyrmion can be stabilized in a BFO slab. We chose to nucleate numerically an individual skyrmion in a box with periodic boundary conditions and let the numerical simulations relax to their equilibrium state. In order for the calculation to be unaffected by the boundaries, we have varied the box size and observe that they converge to a similar energy for a size above 120 nm. The resulting entity is shown in Fig. 3a, where it can be seen that the relaxed skyrmion size is about 30 nm in $BiFeO_3$ (close to half the pitch of the cycloid in the bulk). Interestingly, in a magneto-electric the skyrmion is of hybrid nature as the spin winding generates an extra polarization in virtue of the spin current model: $\overrightarrow{P_{ME}} \sim \overrightarrow{e_{ij}} \times (\vec{S_i} \times \vec{S_j})$. Note that this electrical part of the skyrmion is not chiral as it is generated by the spin chirality in a direction parallel to $\vec{P}$, hence purely along [111]. Moreover, we have also let the simulations converge starting from different initial conditions including a collinear AF state and an infinite cycloid. The results for the phase diagram as a function of the uniaxial anisotropy K_1, show that the energy of the skyrmion state is never the lowest. Indeed, as shown in Fig. 2c, the ground state is found to be the cycloidal one at low K and the collinear AF above K_1 = 0.010 meV. However, for K slightly above 0.010 meV and all the way to 0.020 meV, a skyrmion can be successfully relaxed (Fig. 2a) if the initial state has already the right topology, i.e. if one nucleates a skyrmion in such a material, it is metastable. This can be verified by a procedure called GNEB[15] implemented in the Atomic/Molecular Massively Parallel Simulator LAMMPS[16] (Copyright (2003) Sandia Corporation). It is presented in Fig. 2d for K_1 = 0.012 meV where the minimum energy path is computed for skyrmion annihilation. It is found hereby that in order to unwind the topological structure, an energy barrier of the order of 0.7eV has to be overcome. This is much above what temperature can do and we conclude that once nucleated, these entities are very stable in $BiFeO_3$. Again, the main requirement here is that the uniaxial anisotropy has to be increased compared to that in bulk samples. This seems however reachable by epitaxial strain as it has been shown[17,18] that a resulting induced anisotropy can reach the right order of magnitude to explore the full phase diagram (collinear AF and different cycloid types) when BFO is grown on different substrates with different orientations[18–20].

This project has received funding from the European Union's Horizon 2020 research and innovation programme under grant agreement No 964931

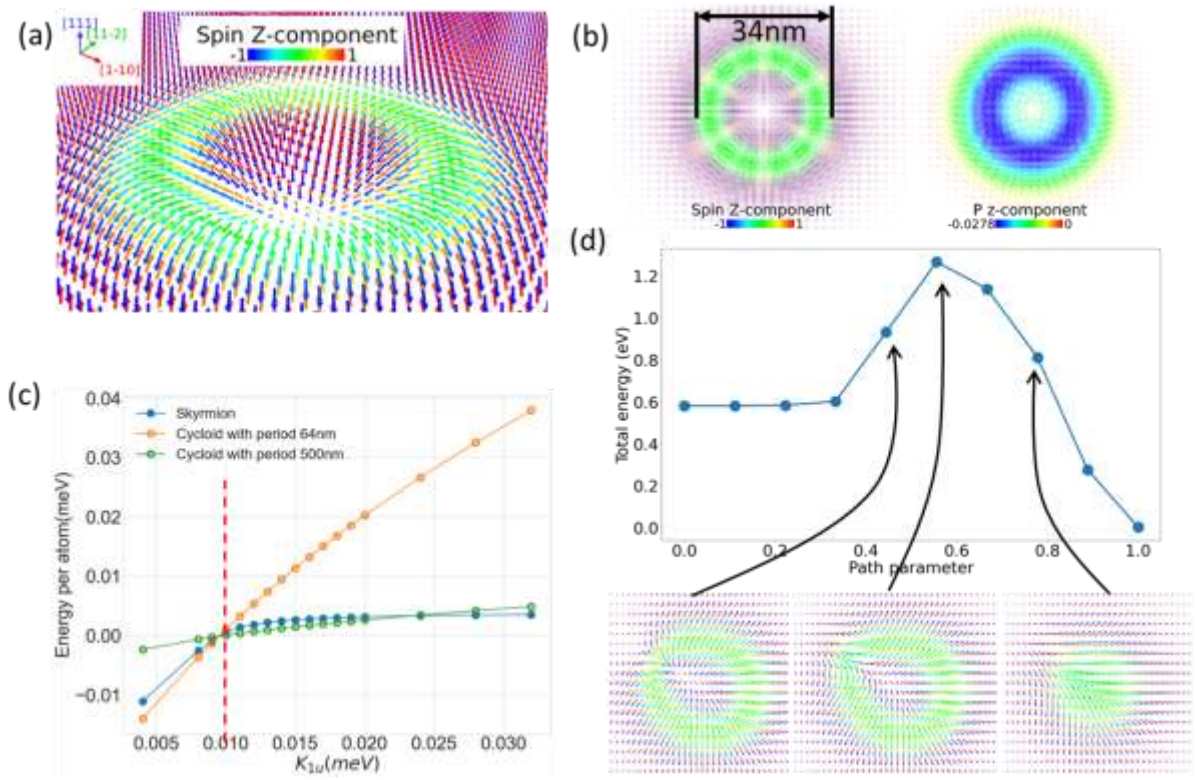

Figure 3: Meta-stability of skyrmionic states. *(a) Relaxed AF skyrmion state for an anisotropy of K=0.012meV. (b) z projection of the spin component (left) and the associated electric polarization (right). (c) Phase diagram (energy vs anisotropy) where the zero is set for the collinear AF state. The obtained ground states are the 64nm cycloid below K=0.010 meV and the collinear AF state above. (d) Unwinding of a skyrmion as obtained with the GNEB technique following the minimum energy path. Skyrmions are metastable but once nucleated, they are protected by a large energy barrier of 0.7eV (for K=0.012meV) of topological nature.*

3) Interfacial DM interaction in antiferromagnetc oxide / heavy metal bilayers

Parallel to these activities, we have also explored the DM interaction at the interface between an antiferromagnetic insulator and an ultrathin heavy metal layer. We have decided to focus on Pt on $LaFeO_3$ (LFO) as shown in Figure 4. This particular configuration was chosen because LFO is a prototypical antiferromagnetic insulator available experimentally in the consortium. It has a high Néel temperature of 750 K and no magnetic ions on the perovskite A site. It also has a relatively small lattice mismatch with Pt. In contrast to BFO, LFO is not ferroelectric. Here the DM interaction is not due to ferroelectricity but to the interface with Pt. The Pt is hybridizing with non-magnetic La and Fe is not subjected to any internal electric field due to the absence of ferroelectricity. Furthermore, Pt is unlikely to hybridize with Fe directly due to the presence of the top LaO layer whose electrons will screen the d- and f-electrons of La.

This project has received funding from the European Union's Horizon 2020 research and innovation programme under grant agreement No 964931

The SOC contribution in this particular composition is shown in figure 5. For this particular sample composition, the SOC contribution was obtained by applying SOC perpendicular to a spin spiral propagating along the high symmetry lines of the 2D cubic Brillouin zone. This DM interaction agrees with the LF model. Although the DM interaction is exactly 0 in the absence of the Pt layer, it reaches up to 2 meV/Fe in the presence of the Pt layer. This value of DM interaction reaches far beyond the one of multiferroics and even metals. It could come from the associated effects of a Rashba-like DM interaction originating from a chemical potential difference between the Pt and LaO layers and a hybridization between the d-orbitals of Fe with the La and Pt d and f orbitals. These results show that the interface between a heavy metal and an insulator might produce a giant DM interaction, which is very promising for future activities planned in TSAR.

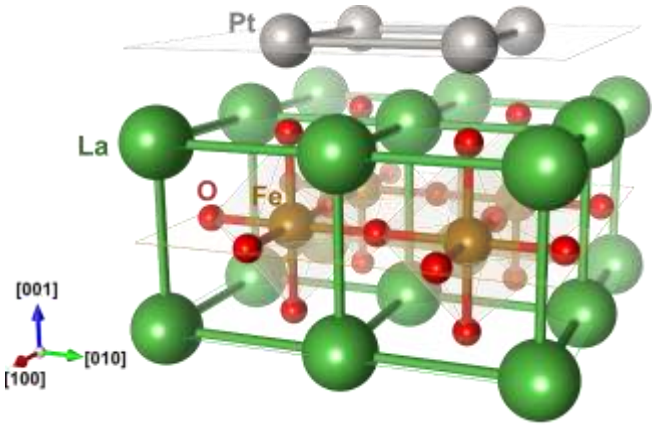

Figure 4: ***Structure of Pt on $LaFeO_3$.*** *In the cubic perovskite $LaFeO_3$, the Dzyaloshinskii-Moriya interaction is zero because the system is centrosymmetric. Adding a layer of Pt on top breaks the inversion symmetry at the interface and hence, a DMI can occur.*

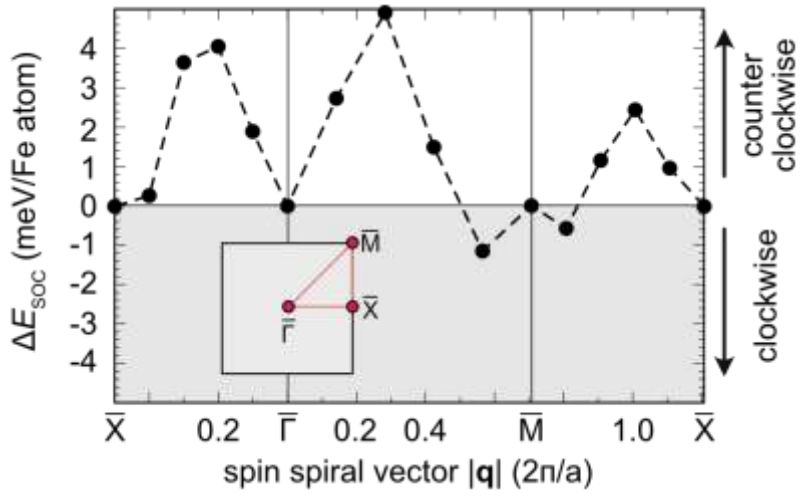

Figure 5: ***DMI in $Pt/LaFeO_3$.*** *Energy contribution due to spin-orbit coupling of flat spin spirals. The Brillouin zone is shown as inset, negative values represent clockwise rotational preference of spin spiral states, positive values counterclockwise rotation. Without the Pt layer on top, the DMI in cubic LFO is zero, with Pt on top, the DMI at the interface reaches up to 2 meV.*

References:

1. Fert, A. *et al.* **Phys. Rev. Lett.** 44, 1538 (1980).
2. Desplat, L. *et al.* **Phys. Rev. B** 104, L060409 (2021).
3. Yang, H. *et al.* **Nature Mater** 17, 605 (2018).
4. He, X. *et al.* **Computer Physics Communications** 264, 107938 (2021).
5. Heide, M. *et al.* **Physica B: Condensed Matter** 404, 2678 (2009).
6. Meyer, S. *et al.* **ArXiv** 2210.15591 (2022) doi:10.48550/arXiv.2210.15591.
7. Fishman, R. S. **Physica B: Condensed Matter** 536, 115 (2018).
8. Soumyanarayanan, A. *et al.* **Nature** 539, 509 (2016).
9. Katsura, H. *et al.* **Phys Rev Lett.** 95, 057205 (2005).
10. Mostovoy, M. **Phys. Rev. Lett.** 96, 067601 (2006).
11. Kadomtseva, A. M. *et al.* **JETP Letters** 79, 571 (2004).
12. Cheng, R. *et al.* **Physical Review Letters** 113, (2014).
13. Cheng, R. *et al.* **Physical Review B** 91, (2015).
14. Chirac, T. *et al.* **Phys. Rev. B** 102, 134415 (2020).
15. Bessarab, P. F. *et al.* **Computer Physics Communications** 196, 335 (2015).
16. Tranchida, J. *et al.* **Journal of Computational Physics** 372, 406 (2018).
17. Haykal, A. *et al.* **Nat Commun** 11, 1704 (2020).
18. Sando, D. *et al.* **Nature Materials** 12, 641 (2013).
19. Chen, Z. *et al.* **Nat Commun** 9, 3764 (2018).
20. Bai, F. *et al.* **Appl. Phys. Lett.** 86, 032511 (2005).

This project has received funding from the European Union's Horizon 2020 research and innovation programme under grant agreement No 964931